Measurement of the time-integrated *CP* asymmetry in $D^0 \to K^0_S K^0_S$ decays using Belle and Belle II data

I. Adachi, L. Aggarwal, H. Ahmed, H. Aihara, N. Akopov, A. Aloisio, N. Althubiti, N. Anh Ky, D. M. Asner, H. Atmacan, V. Aushev, M. Aversano, R. Ayad, V. Babu, N. K. Baghel, S. Bahinipati, P. Bambade, Sw. Banerjee, S. Bansal, M. Barrett, M. Bartl, J. Baudot, A. Beaubien, J. Becker, J. V. Bennett, V. Bertacchi, M. Bertemes, E. Bertholet, M. Bessner, S. Bettarini, B. Bhuyan, D. Biswas, A. Bobrov, D. Bodrov, A. Bolz, A. Boschetti, A. Bozek, M. Bračko, P. Branchini, R. A. Briere, T. E. Browder, A. Budano, S. Bussino, Q. Campagna, M. Campajola, G. Casarosa, C. Cecchi, J. Cerasoli, M.-C. Chang, P. Chang, R. Cheaib, P. Cheema, C. Chen, B. G. Cheon, K. Chilikin, K. Chirapatpimol, H.-E. Cho, K. Cho, S.-J. Cho, S.-K. Choi, S. Choudhury, J. Cochran, L. Corona, J. X. Cui, S. Das, E. De La Cruz-Burelo, S. A. De La Motte, G. De Pietro, R. de Sangro, M. Destefanis, A. Di Canto, F. Di Capua, J. Dingfelder, Z. Doležal, T. V. Dong, M. Dorigo, D. Dossett, G. Dujany, P. Ecker, J. Eppelt, P. Feichtinger, T. Ferber, T. Fillinger, C. Finck, G. Finocchiaro, A. Fodor, F. Forti, B. G. Fulsom, A. Gabrielli, E. Ganiev, G. Gaudino, V. Gaur, A. Gaz, A. Gellrich, G. Ghevondyan, D. Ghosh, H. Ghumaryan, G. Giakoustidis, R. Giordano, A. Giri, P. Gironella Gironell, A. Glazov, B. Gobbo, R. Godang, P. Goldenzweig, W. Gradl, E. Graziani, D. Greenwald, Z. Gruberová, Y. Guan, K. Gudkova, I. Haide, T. Hara, K. Hayasaka, H. Hayashii, S. Hazra, C. Hearty, M. T. Hedges, A. Heidelbach, I. Heredia de la Cruz, M. Hernández Villanueva, T. Higuchi, M. Hoek, M. Hohmann, R. Hoppe, C.-L. Hsu, T. Humair, T. Iijima, K. Inami, N. Ipsita, A. Ishikawa, R. Itoh, M. Iwasaki, W. W. Jacobs, D. E. Jaffe, E.-J. Jang, Q. P. Ji, S. Jia, Y. Jin, A. Johnson, K. K. Joo, H. Junkerkalefeld, A. B. Kaliyar, J. Kandra, G. Karyan, F. Keil, C. Kiesling, C.-H. Kim, D. Y. Kim, J.-Y. Kim, K.-H. Kim, Y.-K. Kim, K. Kinoshita, P. Kodyš, T. Koga, S. Kohani, K. Kojima, A. Korobov, S. Korpar, E. Kovalenko, R. Kowalewski, P. Križan, P. Krokovny, T. Kuhr, K. Kumara, T. Kunigo, A. Kuzmin, Y.-J. Kwon, S. Lacaprara, Y.-T. Lai, K. Lalwani, T. Lam, J. S. Lange, T. S. Lau, M. Laurenza, R. Leboucher, F. R. Le Diberder, M. J. Lee, C. Lemettais, P. Leo, C. Li, L. K. Li, Q. M. Li, W. Z. Li, Y. B. Li, Y. P. Liao, J. Libby, M. H. Liu, Q. Y. Liu, Y. Liu, Z. Q. Liu, D. Liventsev, S. Longo, T. Lueck, C. Lyu, C. Madaan, M. Maggiora, S. P. Maharana, R. Maiti, G. Mancinelli, R. Manfredi, E. Manoni, M. Mantovano, D. Marcantonio, S. Marcello, C. Marinas, C. Martellini, A. Martens, A. Martini, T. Martinov, L. Massaccesi, M. Masuda, D. Matvienko, S. K. Maurya, M. Maushart, J. A. McKenna, R. Mehta, F. Meier, M. Merola, C. Miller, M. Mirra, S. Mitra, K. Miyabayashi, G. B. Mohanty, S. Mondal, S. Moneta, H.-G. Moser, R. Mussa, I. Nakamura, M. Nakao, Y. Nakazawa, M. Naruki, Z. Natkaniec, A. Natochii, M. Nayak, G. Nazaryan, M. Neu, S. Nishida, S. Ogawa, H. Ono, E. R. Oxford, G. Pakhlova, S. Pardi, K. Parham, H. Park, J. Park, K. Park, S.-H. Park, B. Paschen, A. Passeri, S. Patra, T. K. Pedlar, I. Peruzzi, R. Peschke, M. Piccolo, L. E. Piilonen, P. L. M. Podesta-Lerma, T. Podobnik, C. Praz, S. Prell, E. Prencipe, M. T. Prim, H. Purwar, S. Raiz, N. Rauls, J. U. Rehman, M. Reif, S. Reiter, L. Reuter, D. Ricalde Herrmann, I. Ripp-Baudot, G. Rizzo, M. Roehrken, J. M. Roney, A. Rostomyan, N. Rout, D. A. Sanders, S. Sandilya, L. Santelj, V. Savinov, B. Scavino, M. Schnepf, C. Schwanda, Y. Seino, A. Selce, K. Senyo, J. Serrano, M. E. Sevior, C. Sfienti, W. Shan, X. D. Shi, J.-G. Shiu, D. Shtol, B. Shwartz, A. Sibidanov, F. Simon, J. Skorupa, R. J. Sobie, M. Sobotzik, A. Soffer, A. Sokolov, E. Solovieva, S. Spataro, B. Spruck, M. Starič, P. Stavroulakis, S. Stefkova, R. Stroili, J. Strube, M. Sumihama, K. Sumisawa, H. Svidras, M. Takizawa, U. Tamponi, K. Tanida, F. Tenchini, O. Tittel, R. Tiwary, E. Torassa, K. Trabelsi, I. Ueda, T. Uglov, K. Unger, Y. Unno, K. Uno, S. Uno, P. Urquijo, Y. Ushiroda, S. E. Vahsen, R. van Tonder, K. E. Varvell, M. Veronesi, A. Vinokurova, V. S. Vismaya, L. Vitale, V. Vobbilisetti, R. Volpe, M. Wakai, S. Wallner, M.-Z. Wang, A. Warburton, M. Watanabe, S. Watanuki, C. Wessel, E. Won, B. D. Yabsley, S. Yamada, W. Yan, J. Yelton, J. H. Yin, K. Yoshihara, J. Yuan, L. Zani, B. Zhang, V. Zhilich, J. S. Zhou, Q. D. Zhou, L. Zhu, V. I. Zhukova, and R. Žlebčík

(Belle and Belle II Collaborations)

(Received 4 November 2024; accepted 23 December 2024; published 30 January 2025)

We measure the time-integrated CP asymmetry in $D^0 \to K^0_S K^0_S$ decays reconstructed in $e^+e^- \to c\bar{c}$ events collected by the Belle and Belle II experiments. The corresponding data samples have integrated luminosities of 980 and 428 fb^{-1}, respectively. The D^0 decays are required to originate from the $D^{*+} \to D^0\pi^+$ decay, which determines the charm flavor at production time. A control sample of $D^0 \to K^+K^-$ decays is used to correct for production and detection asymmetries. The result, $(-1.4 \pm 1.3(\text{stat}) \pm 0.1(\text{syst}))\%$, is consistent with previous determinations and with CP symmetry.

DOI: 10.1103/PhysRevD.111.012015

I. INTRODUCTION

Charge-parity (CP) violation in the charm sector was first observed by the LHCb Collaboration in the difference between the CP asymmetries of $D^0 \to K^+K^-$ and $D^0 \to \pi^+\pi^-$ decays [1]. (Throughout this paper, charge-conjugate modes are implied unless stated otherwise.) A more recent result reports evidence that the CP violation occurs primarily in the $D^0 \to \pi^+\pi^-$ mode [2]. However, the origin of the LHCb CP asymmetry is not fully understood and there is a debate about whether it could be due to physics beyond the standard model [3–6]. This motivates additional measurements of CP asymmetries in D decays to two pseudoscalars to evaluate predictions based on the pattern of flavor-$SU(3)$ breaking in charm decays [4,7].

The $D^0 \to K^0_S K^0_S$ decay proceeds through a color- and Cabibbo-suppressed transition that involves interference between $c \to us\bar{s}$ and $c \to ud\bar{d}$ amplitudes, mediated by the exchange of a W boson at tree level. Such interference can generate CP asymmetries at the 1% level, even if the Cabibbo-Kobayashi-Maskawa phase is the only source of CP violation [7–9]. These features make the $D^0 \to K^0_S K^0_S$ mode an important ingredient in understanding of the origin of CP violation in charm decays.

Several experiments have searched for CP violation in $D^0 \to K^0_S K^0_S$ decays [10–14]. The world-average value of the CP asymmetry, $A_{CP}(D^0 \to K^0_S K^0_S) = (-1.9 \pm 1.0)\%$ [15], is dominated by measurements from Belle [12] and LHCb [13]. Using a sample of e^+e^- collisions with an integrated luminosity of 921 fb^{-1}, Belle measured $A_{CP}(D^0 \to K^0_S K^0_S) = (-0.02 \pm 1.53 \pm 0.02 \pm 0.17)\%$, where the first uncertainty is statistical, the second systematic, and the third is due to the uncertainty in the CP asymmetry of the $D^0 \to K^0_S\pi^0$ reference mode. A more precise result is obtained by LHCb using a 6 fb^{-1} sample of pp collisions: $(-3.1 \pm 1.2 \pm 0.4 \pm 0.2)\%$, where the first uncertainty is statistical, the second is systematic, and the third is due to the uncertainty in the CP asymmetry of the reference $D^0 \to K^+K^-$ decay. The measurement of $A_{CP}(D^0 \to K^+K^-)$ has been recently improved by LHCb [2], bringing the corresponding uncertainty below the 0.1% level. The precision of the world-average value of $A_{CP}(D^0 \to K^0_S K^0_S)$ is therefore limited by statistical uncertainties and is expected to greatly improve over the next few years with the larger samples being collected at LHCb and Belle II.

In this paper, we report a measurement of $A_{CP}(D^0 \to K^0_S K^0_S)$ using a combination of Belle and Belle II data, which have integrated luminosities of 980 and 428 fb^{-1} [16], respectively. To determine the production flavor of the neutral D meson, which is referred to as "tagging," we reconstruct $D^0 \to K^0_S K^0_S$ decays from $D^{*+} \to D^0\pi^+$ decays in $e^+e^- \to c\bar{c}$ events. The decay-time-integrated CP asymmetry, defined as

$$A_{CP}(D^0 \to K^0_S K^0_S) = \frac{\Gamma(D^0 \to K^0_S K^0_S) - \Gamma(\bar{D}^0 \to K^0_S K^0_S)}{\Gamma(D^0 \to K^0_S K^0_S) + \Gamma(\bar{D}^0 \to K^0_S K^0_S)}, \tag{1}$$

where Γ is the time-integrated decay rate, is measured from the *raw* asymmetry in reconstructed yields,

$$A_{\text{raw}}^{K^0_S K^0_S} = \frac{N(D^0 \to K^0_S K^0_S) - N(\bar{D}^0 \to K^0_S K^0_S)}{N(D^0 \to K^0_S K^0_S) + N(\bar{D}^0 \to K^0_S K^0_S)}, \tag{2}$$

after correcting for "nuisance" asymmetries induced by production and detection mechanisms. The nuisance asymmetries are determined using the control channel $D^{*+} \to D^0(\to K^+K^-)\pi^+$. In the limit of small CP and nuisance asymmetries, the raw asymmetry of a D^{*+}-tagged D^0 decay to a two-body and CP-symmetric final state f can be expressed as

$$A_{\text{raw}}^f = A_{CP}(D^0 \to f) + A_{\text{P}}^{D^{*+}}(D^0 \to f) + A_\epsilon^\pi(D^0 \to f). \tag{3}$$

The term $A_{\text{P}}^{D^{*+}}$ arises, in $e^+e^- \to c\bar{c}$ events, from the forward-backward asymmetric production of charm hadrons due to γ^*-Z^0 interference and higher-order QED

Published by the American Physical Society under the terms of the Creative Commons Attribution 4.0 International license. Further distribution of this work must maintain attribution to the author(s) and the published article's title, journal citation, and DOI. Funded by SCOAP^3.

effects [17–19]. This production asymmetry is an odd function of the cosine of the polar angle in the center of mass system, $\cos\theta^*(D^{*+})$, and therefore averages to zero only when integrated over a $\cos\theta^*(D^{*+})$-symmetric acceptance, which is not the case at Belle and Belle II. The term A_ε^π is the detection asymmetry of the low-momentum tagging pion from the D^{*+} decay ("soft" pion). Having opposite strangeness, the two kaons in the D^0 final states do not contribute any *CP* violation or detection asymmetry. Assuming that the nuisance asymmetries are identical for $D^0 \to K_S^0 K_S^0$ and $D^0 \to K^+K^-$ decays, or that they can be made so by weighting the control sample, the *CP* asymmetry in $D^0 \to K_S^0 K_S^0$ decays can be determined as

$$A_{CP}(D^0 \to K_S^0 K_S^0) = A_{\rm raw}^{K_S^0 K_S^0} - A_{\rm raw}^{K^+K^-} + A_{CP}(D^0 \to K^+K^-), \tag{4}$$

where $A_{CP}(D^0 \to K^+K^-)$ is an external input. In particular, we use $A_{CP}(D^0 \to K^+K^-)$ computed from the results reported in Refs. [2,20] as

$$\begin{aligned} A_{CP}(D^0 \to K^+K^-) &= A_{CP}^{\rm dir}(D^0 \to K^+K^-) + \Delta Y \\ &= (6.7 \pm 5.4) \times 10^{-4}, \end{aligned} \tag{5}$$

where $A_{CP}^{\rm dir}$ is the direct *CP* asymmetry, ΔY is the asymmetry arising from *CP* violation in mixing and in the interference between mixing and decay [21,22], and we have used the fact that the average decay times of the selected $D^0 \to K^+K^-$ decays are equal to the D^0 lifetime. The value of ΔY is here assumed to be independent of the D^0 decay mode [21]. The measurements of $A_{CP}^{\rm dir}(D^0 \to K^+K^-)$ from Ref. [2], $(7.7 \pm 5.7) \times 10^{-4}$, and ΔY from Ref. [20], $(-1.0 \pm 1.1) \times 10^{-4}$, have a total correlation of 35% [23].

To avoid potential bias, an arbitrary and undisclosed offset is added to the measured value of $A_{\rm raw}^{K_S^0 K_S^0}$ from the data. This offset remains undisclosed until we finalize the entire analysis procedure and determine all uncertainties.

The paper is organized as follows. Section II provides an overview of the Belle and Belle II detectors. Section III details the simulation samples used in the measurement. The reconstruction and selection of both the signal $D^0 \to K_S^0 K_S^0$ and control $D^0 \to K^+K^-$ decays are presented in Sec. IV. Section V discusses the weighting of the control mode to match the kinematic distributions of the signal mode and ensure an accurate cancellation of the nuisance asymmetries. Determination of the raw asymmetries is covered in Sec. VI, followed by a discussion of the systematic uncertainties affecting the measurement in Sec. VII. Final results are presented in Sec. VIII, followed by concluding remarks.

II. BELLE AND BELLE II DETECTORS

The Belle experiment [24,25] operated at the KEKB asymmetric-energy e^+e^- collider [26,27] between 1999 and 2010. The detector consisted of a large-solid-angle spectrometer, which included a double-sided silicon-strip vertex detector, a 50-layer central drift chamber, an array of aerogel threshold Cherenkov counters, a barrel-like arrangement of time-of-flight scintillation counters, and an electromagnetic calorimeter composed of CsI(Tl) crystals. All subdetectors were located inside a superconducting solenoid coil that provided a 1.5 T magnetic field. An iron flux-return yoke, placed outside the coil, was instrumented with resistive-plate chambers to detect K_L^0 mesons and identify muons. Two inner detector configurations were used: a 2.0 cm radius beam pipe and a three-layer silicon vertex detector; and, from October 2003, a 1.5 cm radius beam pipe, a four-layer silicon vertex detector, and a small-inner-cell drift chamber [28].

The Belle II detector [29,30] is an upgrade with several new subdetectors designed to handle the significantly larger beam-related backgrounds of the new collider, SuperKEKB [31]. It consists of a silicon vertex detector wrapped around a 1 cm radius beam pipe and comprising two inner layers of pixel detectors and four outer layers of double-sided strip detectors, a 56-layer central drift chamber, a time-of-propagation detector, an aerogel ring-imaging Cherenkov detector, and an electromagnetic calorimeter, all located inside the same solenoid as used for Belle. A flux return outside the solenoid is instrumented with resistive-plate chambers, plastic scintillator modules, and an upgraded readout system to detect muons and K_L^0 mesons. For the data used in this paper, collected between 2019 and 2022, only part of the second layer of the pixel detector, covering 15% of the azimuthal angle, was installed.

III. SIMULATION

We use simulated event samples to identify sources of background, optimize selection criteria, match the kinematic distributions of signal and control decays, determine fit models, and validate the analysis procedure. We generate $e^+e^- \to \Upsilon(nS)$ $(n = 4,\ 5)$ events and simulate particle decays with EvtGen [32]; we generate continuum $e^+e^- \to q\bar{q}$ (where q is a u, d, c, or s quark) with PYTHIA6 [33] for Belle, and with KKMC [34] and PYTHIA8 [35] for Belle II; we simulate final-state radiation with PHOTOS [36,37]; we simulate detector response using Geant3 [38] for Belle and Geant4 [39] for Belle II. In the Belle simulation, beam backgrounds are taken into account by overlaying random trigger data. In the Belle II simulation, they are accounted for by simulating the Touschek effect [40], beam-gas scattering, and luminosity-dependent backgrounds from Bhabha scattering and two-photon QED processes [41,42].

IV. RECONSTRUCTION AND EVENT SELECTION

We use the Belle II analysis software framework (BASF2) to reconstruct both Belle and Belle II data [43,44]. The Belle data are converted to the Belle II format for BASF2 compatibility using the B2BII framework [45].

Events are selected by a trigger based on either the total energy deposited in the electromagnetic calorimeter or the number of charged-particle tracks reconstructed in the central drift chamber. The efficiency of the trigger is found to be close to 100% for both signal and control mode decays.

Candidate $K^0_S \to \pi^+\pi^-$ decays are reconstructed from combinations of oppositely charged particles that are constrained to originate from a common vertex. These particles are assumed to be pions and the resulting di-pion mass is required to be in the $[0.45, 0.55]$ GeV/c^2 range. Pairs of K^0_S candidates are combined to form candidate $D^0 \to K^0_S K^0_S$ decays. The mass of the D^0 candidate, $m(K^0_S K^0_S)$, is required to be in the $[1.85, 1.89]$ GeV/c^2 range for Belle and in the $[1.85, 1.88]$ GeV/c^2 range for Belle II, corresponding to approximately 3 times the mass resolution. The different ranges account for a small offset observed in the D^0 mass-peak positions in the two datasets and for the different mass resolutions.

For the control mode decays, candidate D^0 mesons are formed by combining pairs of oppositely charged kaons with mass, $m(K^+K^-)$, in the $[1.75, 2.05]$ GeV/c^2 range. Tracks originating from charged kaons must have at least 20 hits in the central drift chamber and at least one hit in the silicon vertex detector. They must have a distance of closest approach to the e^+e^- interaction point (IP) smaller than 2.0 cm in the longitudinal direction (parallel to the solenoid axis and in the direction of the positron beam) and smaller than 0.5 cm in the transverse plane. We identify kaons by requiring $\mathcal{L}_K/(\mathcal{L}_K + \mathcal{L}_\pi) > 0.6$ and $\mathcal{L}_K/(\mathcal{L}_K + \mathcal{L}_e) > 0.1$, where $\mathcal{L}_x$ is the likelihood for the hypothesis x to have produced the relevant track. The particle-identification likelihoods are based on information from the aerogel threshold Cherenkov counters, time-of-flight scintillation counters, and the central drift chamber for Belle; and from all subdetectors except the pixel detector for Belle II. The kaon-identification efficiency is above 86% with rates of pion-to-kaon and electron-to-kaon misidentification below 9% and 20%, respectively.

The D^0 candidates for both signal and control modes are then combined with low-momentum pions to form a $D^{*+} \to D^0\pi^+$ decay. The soft-pion tracks must be in the acceptance of the central drift chamber and have longitudinal and transverse distances of closest approach to the IP smaller than 2.0 and 0.5 cm, respectively. To improve signal efficiency, particle identification is not required for the soft-pion candidates. The D^{*+} candidates undergo a kinematic fit [46], which constrains the D^{*+} vertex to the measured position of the IP and the masses of the two K^0_S candidates to the nominal K^0_S mass [47] for the signal mode. Only candidates whose kinematic fits converge with χ^2 probabilities larger than 10^{-3} are retained for further analysis.

The difference between the reconstructed D^{*+} and D^0 masses is required to be smaller than 0.16 GeV/c^2. To suppress events in which the D^{*+} candidate comes from the decay of a B meson, the momentum of the D^{*+} in the e^+e^- center-of-mass system is required to be greater than 2.5 GeV/c. Simulation shows that the remaining contamination from B meson decays amounts to less than one candidate per 1 ab^{-1} of integrated luminosity and is negligible.

V. KINEMATIC WEIGHTING

Because detector- and production-induced asymmetries depend on kinematic properties of the selected D^{*+} candidates, the asymmetry cancellation is realized accurately only if the kinematic distributions in the $D^0 \to K^0_S K^0_S$ and $D^0 \to K^+K^-$ samples are the same. The D^{*+} production asymmetry is expected to vary as a function of the D^{*+} polar angle, $\theta(D^{*+})$; the soft-pion detection asymmetry is expected to vary both as a function of momentum and of polar angle. Because of the differences in the reconstruction and selection of charged and neutral kaons, small differences are present in these distributions for the selected $D^0 \to K^0_S K^0_S$ and $D^0 \to K^+K^-$ candidates (Fig. 1). A weighting procedure is therefore implemented to reduce the observed differences. The ratio of the $\cos\theta(D^{*+})$ distributions of $D^0 \to K^0_S K^0_S$ and $D^0 \to K^+K^-$ decays in simulation is used to determine a smooth curve that provides a candidate-specific weight for the $D^0 \to K^+K^-$ sample in data. Weighting as a function of $\cos\theta(D^{*+})$ also reduces the differences in the other kinematic distributions (Fig. 1). The $D^0 \to K^+K^-$ distributions shown in the remainder of this paper are weighted according to this procedure.

VI. DETERMINATION OF OBSERVED ASYMMETRIES

The asymmetries between the observed yields of D^{*+} and D^{*-} signal candidates are determined using unbinned maximum-likelihood fits to distributions that distinguish signal and control mode decays from background processes. The fit models are assumed to be the same for charm and anticharm mesons. Their functional forms are extracted from either simulation, with parameter values that are adjusted for the data, or from sideband data.

A. Fit to the $D^0 \to K^0_S K^0_S$ sample

There are three components in the fit: signal $D^0 \to K^0_S K^0_S$ decays, peaking background from $D^0 \to K^0_S\pi^+\pi^-$ decays, and nonpeaking background. Nonpeaking background is separated from the other two components using the

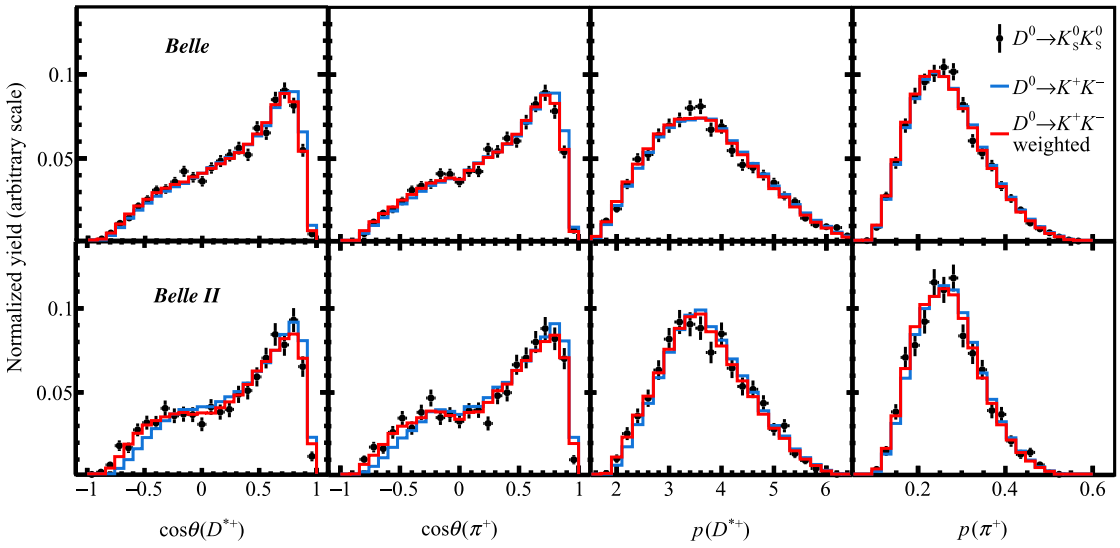

FIG. 1. Normalized distributions of (from left to right) cosine of the D^{*+} polar angle, cosine of the soft-pion polar angle, D^{*+} momentum, and soft-pion momentum of background-subtracted $D^0 \to K^0_S K^0_S$ and $D^0 \to K^+K^-$ decays in (top) Belle and (bottom) Belle II data, before and after the kinematic weighting.

distribution of the D^{*+} mass, $m(D^0\pi^+)$, which is calculated using the vector sum of the momenta of the three final-state particles as D^{*+} momentum, and the known D^0 mass [47] in the determination of the D^{*+} energy [22,48]. Signal and peaking-background $D^0 \to K^0_S\pi^+\pi^-$ decays have identical $m(D^0\pi^+)$ distributions, which narrowly peak at the nominal D^{*+} mass. In contrast, the nonpeaking background has a smooth $m(D^0\pi^+)$ distribution. To separate signal from peaking background, we use the large distance (L) between the K^0_S and D^0 decay vertices resulting from the long K^0_S lifetime. We introduce the variable $S_{\rm min}(K^0_S) = \log\left[\min\left(L_1/\sigma_{L_1}, L_2/\sigma_{L_2}\right)\right]$, where $L_{1(2)}$ and $\sigma_{L_{1(2)}}$ are the distance and its uncertainty for the first (second) K^0_S candidate, respectively. Both the signal and peaking-background $S_{\rm min}(K^0_S)$ distributions exhibit a peaking structure, but they peak at very different values.

We determine the signal yield and raw asymmetry by fitting to the $m(D^0\pi^+)$ and $S_{\rm min}(K^0_S)$ distributions, simultaneously for D^{*+} and D^{*-} candidates. In the fit, the two-dimensional probability density functions (PDFs) of each component can be factorized into the product of one-dimensional PDFs, as verified in simulation. The $m(D^0\pi^+)$ and $S_{\rm min}(K^0_S)$ PDFs of signal and peaking-background decays are each modeled using Johnson's S_U functions with parameters derived from simulation [49]. The $m(D^0\pi^+)$ PDF is assumed to be the same for $D^0 \to K^0_S K^0_S$ and $D^0 \to K^0_S\pi^+\pi^-$ decays; the $S_{\rm min}(K^0_S)$ PDF peaks at larger values for $D^0 \to K^0_S K^0_S$ than for $D^0 \to K^0_S\pi^+\pi^-$ decays. The $m(D^0\pi^+)$ distribution of the nonpeaking background is modeled as a thresholdlike distribution,

$$P^{\rm nonpeak}(m) \propto (m-m_0)^{1/2} + \alpha(m-m_0)^{3/2} \qquad (6)$$

with the threshold parameter m_0 fixed to the known value corresponding to the sum of the nominal D^0 and charged-pion masses [47]. The parameter α is determined directly from the fit to the data, together with the yields and asymmetries of each component. The $S_{\rm min}(K^0_S)$ PDF is modeled as the sum of two Johnson's S_U functions peaking at different values. All the parameter values are determined using candidates populating the $m(D^0\pi^+)$ sideband $[2.005, 2.008] \cup [2.013, 2.023]$ GeV/c^2. Simulation shows that candidates in this sideband reproduce the distribution of the nonpeaking background in the signal region.

The results of the fit to the Belle and Belle II data are shown in Fig. 2. The measured signal yields are 4864 ± 78 in Belle and 2214 ± 51 in Belle II. The raw asymmetry is measured to be $(-1.0 \pm 1.6)\%$ in Belle and $(-0.6 \pm 2.3)\%$ in Belle II. The uncertainties are statistical only. The fit model describes the data well, except for the Belle case in the region around $S_{\rm min}(K^0_S) = 3.5$. The mismodeling is similar for D^{*+} and D^{*-} candidates and hence does not significantly affect the asymmetry. Fits to simulation, which have a similar mismodeling, show no evidence of a bias in the determinations of the signal yield and asymmetry. A systematic uncertainty is assigned by repeating the fit to the data with alternative models, as discussed in Sec. VII.

B. Fit to the $D^0 \to K^+K^-$ sample

The raw asymmetry of the control decays is determined using a fit to the two-dimensional distribution of $m(K^+K^-)$ and $m(D^0\pi^+)$. The fit consists of the following components: $D^0 \to K^+K^-$ control mode decays; $D^0 \to K^-\pi^+$ decays in which the pion is misidentified as a kaon, peaking

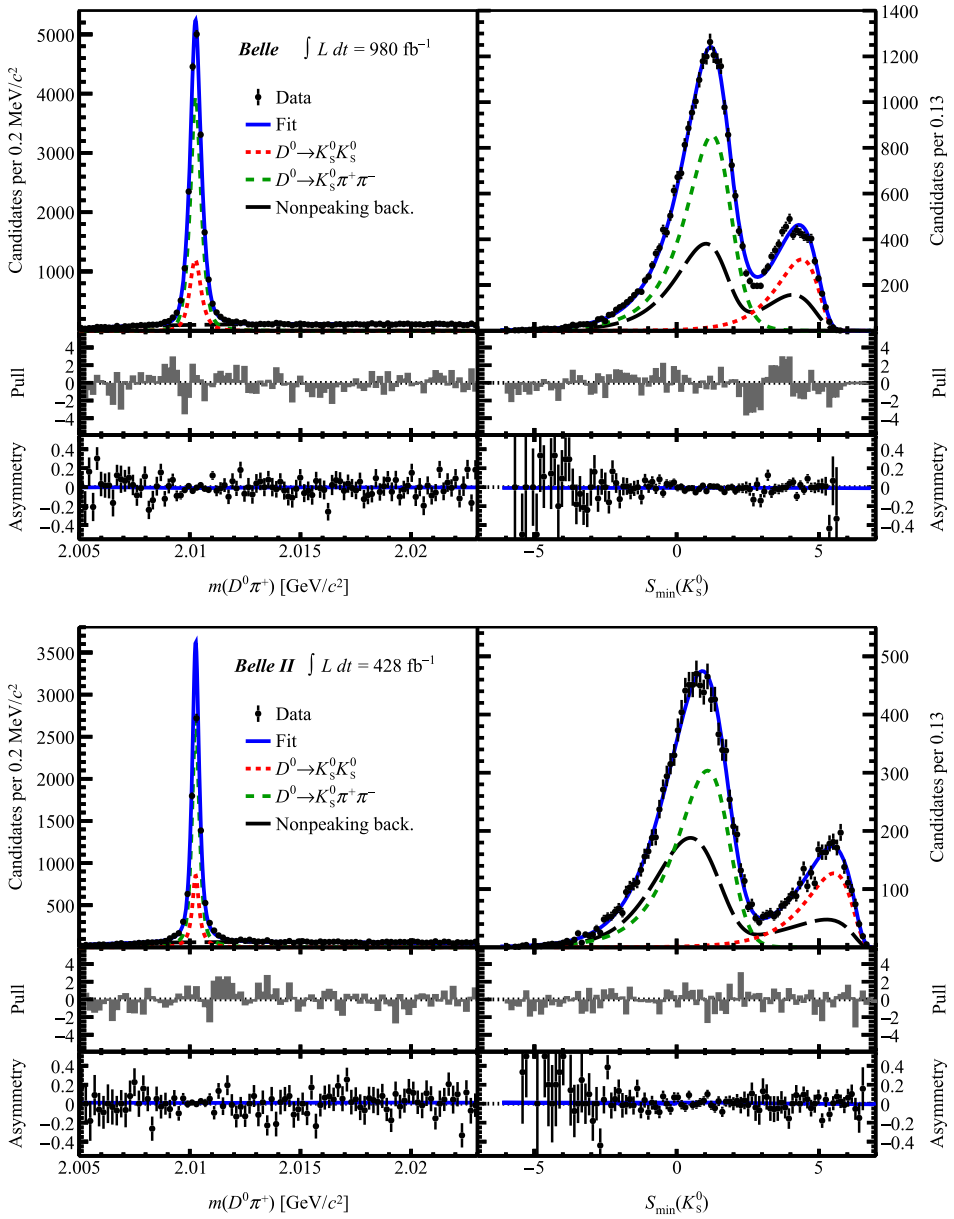

FIG. 2. Distributions of (left) $m(D^0\pi^+)$ and (right) $S_{\min}(K^0_S)$ for combined $D^0 \to K^0_S K^0_S$ and $\bar{D}^0 \to K^0_S K^0_S$ candidates, in (top) Belle and (bottom) Belle II data, with fit projections overlaid. The middle panel of each plot shows the distribution of the difference between observed and fit values divided by the uncertainty from the fit (pull), the bottom panel shows the asymmetry between D^0 and $\bar{D}^0$ candidates with the fit projection overlaid.

at $m(K^+K^-)$ values around 1.94 GeV/c^2; partially reconstructed $D^0 \to$ multibody decays, where the term multibody refers to decays such as $D^0 \to K^-\pi^+\pi^0$, where the charged pion is misidentified as a kaon and the neutral pion is not reconstructed, or semileptonic D^0 decays, where the neutrino is not reconstructed, populating mostly the low-$m(K^+K^-)$ region; $D_s^+ \to K^+K^-\pi^+$ decays in which the π^+ is reconstructed as a soft-pion candidate, peaking at $m(K^+K^-)$ values around 1.82 GeV/c^2; and combinatorial background populating the entire $m(K^+K^-)$ range nearly uniformly. Each D^0 component can either be associated with a real soft-pion candidate, which peaks in $m(D^0\pi^+)$, or with an unrelated soft-pion candidate, which contributes to a smoothly distributed random-pion background in $m(D^0\pi^+)$. The D_s^+ background has a distribution that rises almost linearly in $m(D^0\pi^+)$. Simulation shows that the two-dimensional PDF of each component, except for the $D_s^+ \to K^+K^-\pi^+$ background, can be approximated by the product of two one-dimensional PDFs.

The control decays and physics backgrounds PDFs are determined using simulation. The $m(K^+K^-)$ and $m(D^0\pi^+)$ PDFs of the $D^{*+} \to D^0(\to K^+K^-)\pi^+$ decays are each

modeled using the sum of two Gaussian functions (with a common mean) and of a Johnson's S_U function. The $m(K^+K^-)$ PDF of the misidentified $D^{*+} \to D^0(\to K^-\pi^+)\pi^+$ background is parametrized using the sum of a Gaussian and a Johnson's S_U function. Given that $m(D^0\pi^+)$ is unaffected by the misidentification of the D^0 final-state particles, the $m(D^0\pi^+)$ PDF is shared with that of the control decays. To account for mismodeling of the simulation, shape parameters related to the peak positions and resolutions of the $D^0 \to K^+K^-$ and $D^0 \to K^-\pi^+$ components are floated when fitting to the data, while other parameters are fixed to the values obtained from simulation.

The partially reconstructed $D^{*+} \to D^0(\to \text{multibody})\pi^+$ decays are modeled as an exponential function in $m(K^+K^-)$ and as a Johnson's S_U function in $m(D^0\pi^+)$, with parameters fixed to simulation.

For each of the aforementioned components there is a background in which an unrelated soft pion is associated with the identified D^0 candidate. These random-pion components share the same $m(K^+K^-)$ distribution as the component with the correctly reconstructed soft pion. Their $m(D^0\pi^+)$ distributions are modeled by the following common PDF:

$$P^{\text{rnd}}(m|m_0,A,B) \propto \left[1-\exp\left(-\frac{m-m_0}{A}\right)\right]\left(\frac{m}{m_0}\right)^B, \quad (7)$$

with the parameters A and B free to float in the fit.

The $D_s^+ \to K^+K^-\pi^+$ background, in which the pion is used as the soft-pion candidate, exhibits a kinematic correlation between the average values of $m(K^+K^-)$ and $m(D^0\pi^+)$ which can be calculated analytically as $\langle m(K^+K^-)\rangle(m(D^0\pi^+)) = m_{D_s^+} + m_{D^0} - m(D^0\pi^+)$, using the known D_s^+ and D^0 masses [47]. The two-dimensional PDF is written as the product of the $m(K^+K^-)$ PDF, conditional on the value of $m(D^0\pi^+)$, and the $m(D^0\pi^+)$ PDF,

$$\begin{aligned} &P^{D_s^+}(m(K^+K^-),m(D^0\pi^+)) \\ &\quad = P^{D_s^+}(m(K^+K^-)|m(D^0\pi^+))P^{D_s^+}(m(D^0\pi^+)). \end{aligned} \quad (8)$$

The first term on the right-hand side is parametrized as a Johnson's S_U function with a mean given by $\mu_J + \langle m(K^+K^-)\rangle(m(D^0\pi^+))$, where μ_J is an offset which accounts for possible data-simulation differences in the peak position and is floated in the fit to the data. The $m(D^0\pi^+)$ PDF is a first-order polynomial defined only above the threshold value of m_0.

Finally, the combinatorial background PDF is modeled by a product of a linear function in $m(K^+K^-)$ and Eq. (7) for $m(D^0\pi^+)$. The parameters of the combinatorial background are floated in the fit to the data. The yield and asymmetry of each component are the remaining free parameters of the fit.

The results of the fit to the Belle and Belle II data are shown in Fig. 3. The measured K^+K^- yields are 308760 ± 570 in Belle and 145520 ± 400 in Belle II. The K^+K^- raw asymmetry is measured to be $(0.17 \pm 0.19)\%$ in Belle and $(1.61 \pm 0.27)\%$ in Belle II. The uncertainties are statistical only. The raw-asymmetry values for Belle and Belle II are consistent with expected differences in reconstruction asymmetries for low-momentum pions between the two experiments. While the variation of the asymmetry as a function of the fitted observables is fairly well described by the fit model, the *CP*-averaged distributions of the fitted observables are not. A similar mismodeling is observed in simulation and results in 0.1%–2% biases in the measured K^+K^- yields. The mismodeling has a small effect on the measured asymmetries, as observed in simulation and quantified by refitting to the data with alternative models (Sec. VII).

VII. SYSTEMATIC UNCERTAINTIES

The following sources of systematic uncertainties are considered: PDF modeling in the $D^0 \to K^0_S K^0_S$ and $D^0 \to K^+K^-$ fits, kinematic weighting of the control and signal sample for the cancellation of the nuisance asymmetries, uncertainties on the external input value of $A_{CP}(D^0 \to K^+K^-)$. A summary of the estimated uncertainties is given in Table I, the total is the sum in quadrature of the individual components.

To estimate the systematic uncertainty due to the fit models, we repeat the fit to the data using several variations of the default models. We test two classes of variations: one in which we vary the PDF model, which is the same for D^0 and $\bar{D}^0$ candidates, and another in which we keep the default PDF model but introduce different shape parameters for D^0 and $\bar{D}^0$ candidates. For the first class of variations we use (six for $D^0 \to K^0_S K^0_S$ and seven for $D^0 \to K^+K^-$) alternative models featuring similar or much worse description of the data compared to the default model. The alternative models change the $-2\log\mathcal{L}$ value, where $\mathcal{L}$ is the likelihood at the minimum, by an amount ranging between -6 and 86 for the $K^0_S K^0_S$ fits and between -377×10^3 and 35.9×10^3 for the K^+K^- fits, while having similar numbers of free parameters as the nominal model. The largest variations in the measured raw asymmetries are assigned as systematic uncertainties. From the second class of model variations we observe no significant changes in the asymmetries and consistent fit qualities for alternative and default models. Hence, we assign no additional systematic uncertainty due to the default-fit assumption that D^0 and $\bar{D}^0$ shapes are the same.

The kinematic weighting of the $D^0 \to K^+K^-$ control sample does not entirely remove all differences observed in the D^{*+} and soft-pion momentum and polar angle

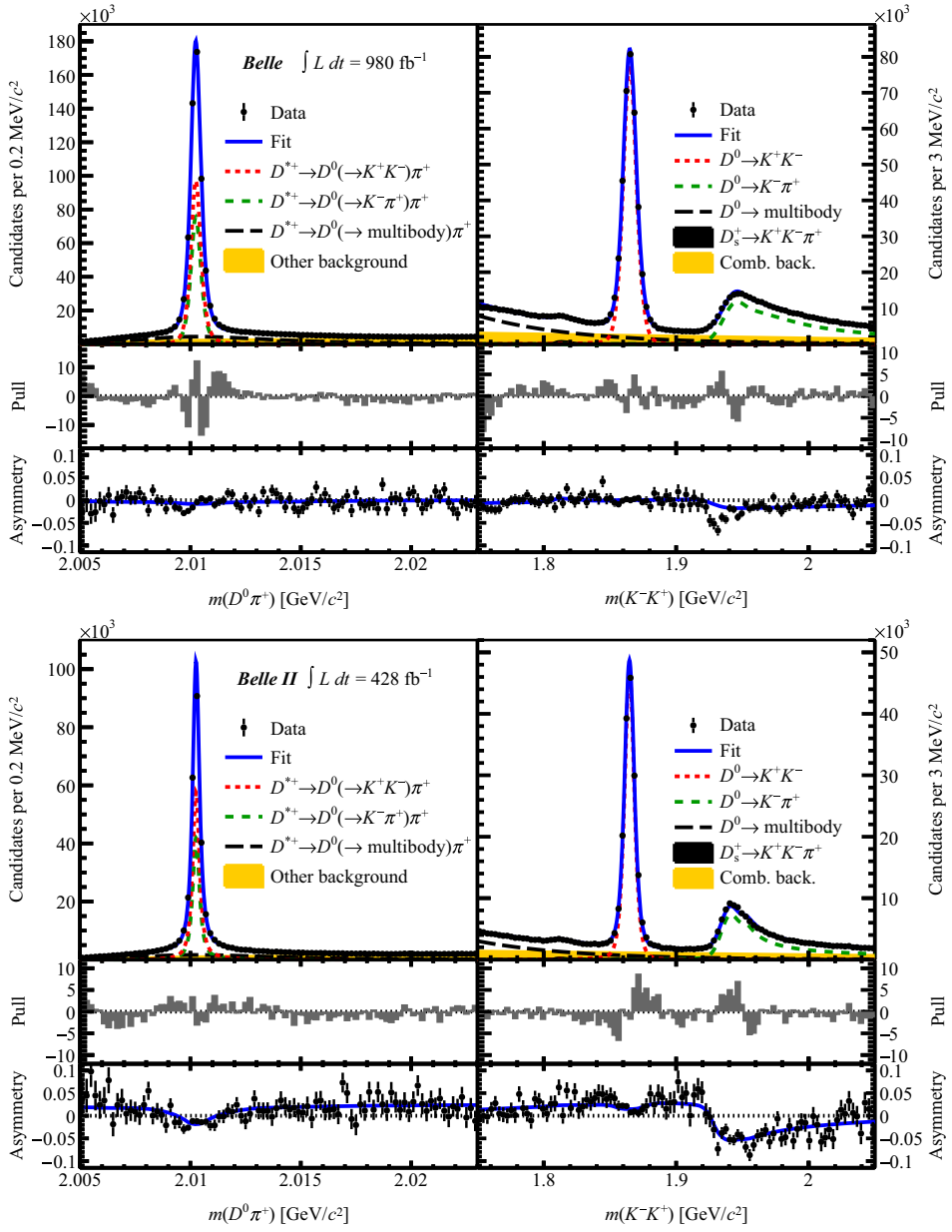

FIG. 3. Distributions of (left) $m(D^0\pi^+)$ and (right) $m(K^+K^-)$ for combined $D^0 \to K^+K^-$ and $\bar{D}^0 \to K^+K^-$ candidates, in (top) Belle and (bottom) Belle II data, with fit projections overlaid. The middle panel of each plot shows the distribution of the difference between observed and fit values divided by the uncertainty from the fit (pull), the bottom panel shows the asymmetry between D^0 and $\bar{D}^0$ candidates with the fit projection overlaid. Other backgrounds include the $D_s^+ \to K^+K^-\pi^+$, random-pion, and combinatorial components.

distributions. The residual differences are approximately a factor 2 smaller than those observed before the weighting. We therefore take half the variation in $A_{\rm raw}^{K^+K^-}$ introduced by the weighting procedure, 0.06% in Belle and 0.07% in Belle II, as a systematic uncertainty.

The uncertainty in the input value of $A_{CP}(D^0 \to K^+K^-)$, 0.05% [Eq. (5)], is propagated as a systematic uncertainty on the measurement.

The entire analysis procedure, including the kinematic weighting of the control mode, is validated using sets of pseudoexperiments generated by sampling from the fit PDFs and using fully simulated decays. In both cases, the results of the validation confirm that we estimate the *CP* asymmetry in $D^0 \to K_S^0K_S^0$ decays, and its uncertainty, without bias.

Finally, we check the consistency of the measured value of $A_{CP}(D^0 \to K_S^0K_S^0)$ by repeating the measurement in disjoint subsets of the data split according to data-taking conditions or momentum of the D^{*+} candidate. In all cases, observed variations in the results are consistent with each other and with the measurement from the full sample.

TABLE I. Summary of uncertainties in $A_{CP}(D^0 \to K^0_S K^0_S)$.

	Uncertainty (%)	
Source	Belle	Belle II
Modeling in the $D^0 \to K^0_S K^0_S$ fit	0.04	0.05
Modeling in the $D^0 \to K^+K^-$ fit	0.02	<0.01
Kinematic weighting	0.06	0.07
Input $A_{CP}(D^0 \to K^+K^-)$	0.05	0.05
Total systematic	0.09	0.10
Statistical	1.60	2.30

VIII. FINAL RESULTS AND CONCLUSIONS

Using D^{*+}-tagged $D^0 \to K^0_S K^0_S$ and $D^0 \to K^+K^-$ decays reconstructed in 980 fb^{-1} of Belle data, and in 428 fb^{-1} of Belle II data, we measure the time-integrated *CP* asymmetry in $D^0 \to K^0_S K^0_S$ decays to be

$$A_{CP}(D^0 \to K^0_S K^0_S) = (-1.1 \pm 1.6(\text{stat}) \pm 0.1(\text{syst}))\% \quad (9)$$

and

$$A_{CP}(D^0 \to K^0_S K^0_S) = (-2.2 \pm 2.3(\text{stat}) \pm 0.1(\text{syst}))\%, \quad (10)$$

respectively. The two results are consistent and agree with previous determinations [10–14]. The result based on Belle data supersedes the published result [12]. It has a factor of 2 smaller systematic uncertainty compared to the previous result thanks to the usage of the $D^0 \to K^+K^-$ control mode, which provides a more precise A_{CP} external input compared to the $D^0 \to K^0_S \pi^0$ control mode used in Ref. [12]. Assuming that the only source of correlation between the two results is the external input value of $A_{CP}(D^0 \to K^+K^-)$, we combine our Belle and Belle II results to obtain

$$A_{CP}(D^0 \to K^0_S K^0_S) = (-1.4 \pm 1.3(\text{stat}) \pm 0.1(\text{syst}))\%. \quad (11)$$

The combined result has precision comparable to the world's best measurement from LHCb [13], with which it agrees.

ACKNOWLEDGMENTS

This work, based on data collected using the Belle II detector, which was built and commissioned prior to March 2019, and data collected using the Belle detector, which was operated until June 2010, was supported by Higher Education and Science Committee of the Republic of Armenia Grant No. 23LCG-1C011; Australian Research Council and Research Grants No. DP200101792, No. DP210101900, No. DP210102831, No. DE220100462, No. LE210100098, and No. LE230100085; Austrian Federal Ministry of Education, Science and Research, Austrian Science Fund (FWF) [Grants DOI: 10.55776/P34529, DOI: 10.55776/J4731, DOI: 10.55776/J4625, and DOI: 10.55776/M3153], and Horizon 2020 ERC Starting Grant No. 947006 "InterLeptons"; Natural Sciences and Engineering Research Council of Canada, Compute Canada and CANARIE; National Key R&D Program of China under Contract No. 2022YFA1601903, National Natural Science Foundation of China and Research Grants No. 11575017, No. 11761141009, No. 11705209, No. 11975076, No. 12135005, No. 12150004, No. 12161141008, No. 12475093, and No. 12175041, and Shandong Provincial Natural Science Foundation Project ZR2022JQ02; the Czech Science Foundation Grant No. 22-18469S and Charles University Grant Agency project No. 246122; European Research Council, Seventh Framework PIEF-GA-2013-622527, Horizon 2020 ERC-Advanced Grants No. 267104 and No. 884719, Horizon 2020 ERC-Consolidator Grant No. 819127, Horizon 2020 Marie Sklodowska-Curie Grant Agreement No. 700525 "NIOBE" and No. 101026516, and Horizon 2020 Marie Sklodowska-Curie RISE project JENNIFER2 Grant Agreement No. 822070 (European grants); L'Institut National de Physique Nucléaire et de Physique des Particules (IN2P3) du CNRS and L'Agence Nationale de la Recherche (ANR) under Grant No. ANR-21-CE31-0009 (France); BMBF, DFG, HGF, MPG, and AvH Foundation (Germany); Department of Atomic Energy under Project Identification No. RTI 4002, Department of Science and Technology, and UPES SEED funding programs No. UPES/R&D-SEED-INFRA/17052023/01 and No. UPES/R&D-SOE/20062022/06 (India); Israel Science Foundation Grant No. 2476/17, U.S.-Israel Binational Science Foundation Grant No. 2016113, and Israel Ministry of Science Grant No. 3-16543; Istituto Nazionale di Fisica Nucleare and the Research Grants BELLE2; Japan Society for the Promotion of Science, Grant-in-Aid for Scientific Research Grants No. 16H03968, No. 16H03993, No. 16H06492, No. 16K05323, No. 17H01133, No. 17H05405, No. 18K03621, No. 18H03710, No. 18H05226, No. 19H00682, No. 20H05850, No. 20H05858, No. 22H00144, No. 22K14056, No. 22K21347, No. 23H05433, No. 26220706, and No. 26400255, and the Ministry of Education, Culture, Sports, Science, and Technology (MEXT) of Japan; National Research Foundation (NRF) of Korea Grants No. 2016R1-D1A1B-02012900, No. 2018R1-A6A1A-06024970, No. 2021R1-A6A1A-03043957, No. 2021R1-F1A-1060423, No. 2021R1-F1A-1064008, No. 2022R1-A2C-1003993, No. 2022R1-A2C-1092335, No. RS-2023-00208693, No. RS-2024-00354342, and No. RS-2022-00197659, Radiation Science Research Institute, Foreign Large-Size Research Facility Application Supporting project, the Global Science Experimental Data Hub Center, the Korea Institute of Science and Technology Information (K24L2M1C4) and KREONET/GLORIAD; Universiti

Malaya RU grant, Akademi Sains Malaysia, and Ministry of Education Malaysia; Frontiers of Science Program Contracts No. FOINS-296, No. CB-221329, No. CB-236394, No. CB-254409, and No. CB-180023, and SEP-CINVESTAV Research Grant No. 237 (Mexico); the Polish Ministry of Science and Higher Education and the National Science Center; the Ministry of Science and Higher Education of the Russian Federation and the HSE University Basic Research Program, Moscow; University of Tabuk Research Grants No. S-0256-1438 and No. S-0280-1439 (Saudi Arabia); Slovenian Research Agency and Research Grants No. J1-9124 and No. P1-0135; Ikerbasque, Basque Foundation for Science, the State Agency for Research of the Spanish Ministry of Science and Innovation through Grant No. PID2022-136510NB-C33, Agencia Estatal de Investigacion, Spain Grant No. RYC2020-029875-I and Generalitat Valenciana, Spain Grant No. CIDEGENT/2018/020; the Swiss National Science Foundation; The Knut and Alice Wallenberg Foundation (Sweden), Contracts No. 2021.0174 and No. 2021.0299; National Science and Technology Council, and Ministry of Education (Taiwan); Thailand Center of Excellence in Physics; TUBITAK ULAKBIM (Turkey); National Research Foundation of Ukraine, Project No. 2020.02/0257, and Ministry of Education and Science of Ukraine; the U.S. National Science Foundation and Research Grants No. PHY-1913789 and No. PHY-2111604, and the U.S. Department of Energy and Research Awards No. DE-AC06-76RLO1830, No. DE-SC0007983, No. DE-SC0009824, No. DE-SC0009973, No. DE-SC0010007, No. DE-SC0010073, No. DE-SC0010118, No. DE-SC0010504, No. DE-SC0011784, No. DE-SC0012704, No. DE-SC0019230, No. DE-SC0021274, No. DE-SC0021616, No. DE-SC0022350, No. DE-SC0023470; and the Vietnam Academy of Science and Technology (VAST) under Grants No. NVCC.05.12/22-23 and No. DL0000.02/24-25. These acknowledgements are not to be interpreted as an endorsement of any statement made by any of our institutes, funding agencies, governments, or their representatives. We thank the SuperKEKB team for delivering high-luminosity collisions; the KEK cryogenics group for the efficient operation of the detector solenoid magnet and IBBelle on site; the KEK Computer Research Center for on-site computing support; the NII for SINET6 network support; and the raw-data centers hosted by BNL, DESY, GridKa, IN2P3, INFN, PNNL/EMSL, and the University of Victoria.

DATA AVAILABILITY

The data that support the findings of this article are not publicly available because of legal restrictions preventing unrestricted public distribution. The data are available from the authors upon reasonable request.

[1] R. Aaij *et al.* (LHCb Collaboration), Observation of *CP* violation in charm decays, Phys. Rev. Lett. **122**, 211803 (2019).

[2] R. Aaij *et al.* (LHCb Collaboration), Measurement of the time-integrated *CP* asymmetry in $D^0 \to K^+K^-$ decays, Phys. Rev. Lett. **131**, 091802 (2023).

[3] M. Chala, A. Lenz, A. V. Rusov, and J. Scholtz, ΔA_{CP} within the standard model and beyond, J. High Energy Phys. 07 (2019) 161.

[4] Y. Grossman and S. Schacht, The emergence of the $\Delta U = 0$ rule in charm physics, J. High Energy Phys. 07 (2019) 020.

[5] S. Schacht and A. Soni, Enhancement of charm *CP* violation due to nearby resonances, Phys. Lett. B **825**, 136855 (2022).

[6] S. Schacht, A *U*-spin anomaly in charm *CP* violation, J. High Energy Phys. 03 (**2023**) 205.

[7] F. Buccella, A. Paul, and P. Santorelli, $SU(3)_F$ breaking through final state interactions and *CP* asymmetries in $D \to PP$ decays, Phys. Rev. D **99**, 113001 (2019).

[8] J. Brod, A. L. Kagan, and J. Zupan, Size of direct *CP* violation in singly Cabibbo-suppressed *D* decays, Phys. Rev. D **86**, 014023 (2012).

[9] U. Nierste and S. Schacht, *CP* violation in $D^0 \to K^0_S K^0_S$, Phys. Rev. D **92**, 054036 (2015).

[10] G. Bonvicini *et al.* (CLEO Collaboration), Search for *CP* violation in $D^0 \to K^0_S\pi^0$ and $D^0 \to \pi^0\pi^0$ and $D^0 \to K^0_S K^0_S$ decays, Phys. Rev. D **63**, 071101 (2001).

[11] R. Aaij *et al.* (LHCb Collaboration), Measurement of the time-integrated *CP* asymmetry in $D^0 \to K^0_S K^0_S$ decays, J. High Energy Phys. 10 (**2015**) 055.

[12] N. Dash *et al.* (Belle Collaboration), Search for *CP* violation and measurement of the branching fraction in the decay $D^0 \to K^0_S K^0_S$, Phys. Rev. Lett. **119**, 171801 (2017).

[13] R. Aaij *et al.* (LHCb Collaboration), Measurement of *CP* asymmetry in $D^0 \to K^0_S K^0_S$ decays, Phys. Rev. D **104**, L031102 (2021).

[14] A. Hayrapetyan *et al.* (CMS Collaboration), Search for *CP* violation in $D^0 \to K^0_S K^0_S$ decays in proton-proton collisions at $\sqrt{s} = 13$ TeV, Eur. Phys. J. C **84**, 1264 (2024).

[15] Y. S. Amhis *et al.* (HFLAV Collaboration), Averages of *b*-hadron, *c*-hadron, and τ-lepton properties as of 2021, Phys. Rev. D **107**, 052008 (2023).

[16] I. Adachi *et al.* (Belle II Collaboration), Measurement of the integrated luminosity of data samples collected during

2019–2022 by the Belle II experiment, Chin. Phys. C **49**, 013001 (2025).
[17] F. A. Berends, K. J. F. Gaemers, and R. Gastmans, α^3 contribution to the angular asymmetry in $e^+e^- \to \mu^+\mu^-$, Nucl. Phys. **B63**, 381 (1973).
[18] R. W. Brown, K. O. Mikaelian, V. K. Cung, and E. A. Paschos, Electromagnetic background in the search for neutral weak currents via $e^+e^- \to \mu^+\mu^-$, Phys. Lett. **43B**, 403 (1973).
[19] R. J. Cashmore, C. M. Hawkes, B. W. Lynn, and R. G. Stuart, The forward-backward asymmetry in $e^+e^- \to \mu^+\mu^-$ comparisons between the theoretical calculations at the one loop level in the standard model and with the experimental measurements, Z. Phys. C **30**, 125 (1986).
[20] R. Aaij *et al.* (LHCb Collaboration), Search for time-dependent *CP* violation in $D^0 \to K^+K^-$ and $D^0 \to \pi^+\pi^-$ decays, Phys. Rev. D **104**, 072010 (2021).
[21] Y. Grossman, A. L. Kagan, and Y. Nir, New physics and *CP* violation in singly Cabibbo suppressed *D* decays, Phys. Rev. D **75**, 036008 (2007).
[22] T. Aaltonen *et al.* (CDF Collaboration), Measurement of *CP*-violating asymmetries in $D^0 \to \pi^+\pi^-$ and $D^0 \to K^+K^-$ decays at CDF, Phys. Rev. D **85**, 012009 (2012).
[23] S. Maccolini (private communication).
[24] A. Abashian *et al.* (Belle Collaboration), The Belle detector, Nucl. Instrum. Methods Phys. Res., Sect. A **479**, 117 (2002).
[25] J. Brodzicka *et al.* (Belle Collaboration), Physics achievements from the Belle experiment, Prog. Theor. Exp. Phys. **2012**, 04D001 (2012).
[26] S. Kurokawa *et al.*, Overview of the KEKB accelerators, Nucl. Instrum. Methods Phys. Res., Sect. A **449**, 1 (2003).
[27] T. Abe *et al.*, Achievements of KEKB, Prog. Theor. Exp. Phys. **2013**, 03A001 (2013).
[28] Z. Natkaniec *et al.*, Status of the Belle silicon vertex detector, Nucl. Instrum. Methods Phys. Res., Sect. A **560**, 1 (2006).
[29] T. Abe *et al.* (Belle II Collaboration), Belle II technical design report, arXiv:1011.0352.
[30] W. Altmannshofer *et al.*, The Belle II physics book, Prog. Theor. Exp. Phys. **2019**, 123C01 (2019); **2020**, 029201(E) (2020).
[31] K. Akai, K. Furukawa, and H. Koiso, SuperKEKB collider, Nucl. Instrum. Methods Phys. Res., Sect. A **907**, 188 (2018).
[32] D. J. Lange, The EvtGen particle decay simulation package, Nucl. Instrum. Methods Phys. Res., Sect. A **462**, 152 (2001).
[33] T. Sjostrand, S. Mrenna, and P. Z. Skands, PYTHIA 6.4 physics and manual, J. High Energy Phys. 05 (2006) 026.
[34] S. Jadach, J. H. Kuhn, and Z. Wąs, TAUOLA: A library of Monte Carlo programs to simulate decays of polarized tau leptons, Comput. Phys. Commun. **64**, 275 (1990).
[35] T. Sjöstrand, S. Ask, J. R. Christiansen, R. Corke, N. Desai, P. Ilten, S. Mrenna, S. Prestel, C. O. Rasmussen, and P. Z. Skands, An introduction to PYTHIA 8.2, Comput. Phys. Commun. **191**, 159 (2015).
[36] E. Barberio, B. van Eijk, and Z. Wąs, PHOTOS: A universal Monte Carlo for QED radiative corrections in decays, Comput. Phys. Commun. **66**, 115 (1991).
[37] E. Barberio and Z. Wąs, PHOTOS: A universal Monte Carlo for QED radiative corrections. Version 2.0, Comput. Phys. Commun. **79**, 291 (1994).
[38] R. Brun *et al.*, Geant: Detector description and simulation tool; 1994, CERN Program Library, CERN, Geneva, 1993.
[39] S. Agostinelli *et al.* (GEANT4 Collaboration), Geant4: A simulation toolkit, Nucl. Instrum. Methods Phys. Res., Sect. A **506**, 250 (2003).
[40] C. Bernardini, G. F. Corazza, G. Di Giugno, G. Ghigo, J. Haissinski, P. Marin, R. Querzoli, and B. Touschek, Lifetime and beam size in a storage ring, Phys. Rev. Lett. **10**, 407 (1963).
[41] P. M. Lewis *et al.*, First measurements of beam backgrounds at SuperKEKB, Nucl. Instrum. Methods Phys. Res., Sect. A **914**, 69 (2019).
[42] A. Natochii *et al.*, Measured and projected beam backgrounds in the Belle II experiment at the SuperKEKB collider, Nucl. Instrum. Methods Phys. Res., Sect. A **1055**, 168550 (2023).
[43] T. Kuhr *et al.* (Belle II Framework Software Group), The Belle II core software, Comput. Software Big Sci. **3**, 1 (2019).
[44] Belle II Collaboration, Belle II Analysis Software Framework (BASF2), 10.5281/zenodo.5574115.
[45] M. Gelb *et al.*, B2BII: Data conversion from Belle to Belle II, Comput. Software Big Sci. **2**, 9 (2018).
[46] J.-F. Krohn *et al.* (Belle II Analysis Software Group), Global decay chain vertex fitting at Belle II, Nucl. Instrum. Methods Phys. Res., Sect. A **976**, 164269 (2020).
[47] S. Navas *et al.* (Particle Data Group), Review of particle physics, Phys. Rev. D **110**, 030001 (2024).
[48] A. Di Canto, Measurement of *CP*-violating asymmetries in $D^0 \to \pi^+\pi^-$ and $D^0 \to K^+K^-$ decays at CDF, Ph.D. thesis, Pisa University, 2012.
[49] N. L. Johnson, Systems of frequency curves generated by methods of translation, Biometrika **36**, 149 (1949).